УДК 621.396.67

ПОЛЯРИЗАТОР ЦИРКУЛЯРНО-ПОЛЯРИЗОВАННОГО СВЧ ИЗЛУЧЕНИЯ НА ОСНОВЕ ДВУХСПИРАЛЬНЫХ ЧАСТИЦ

А.П. Балмаков[1,2], И.В. Семченко[2], С.А. Хахомов[2], М. Нагатсу[1]

[1]*Университет Шизуока, Хамамацу, Япония*
[2]*Гомельский государственный университет им. Ф. Скорины, Гомель, Беларусь*

MICROWAVE CIRCULAR POLARIZER BASED ON BIFILAR HELICAL PARTICLES

A.P. Balmakov[1,2], I.V. Semchenko[2], S.A. Khakhomov[2], M. Nagatsu[1]

[1]*Shizuoka University, Hamamatsu, Japan*
[2]*F. Scorina Gomel State University, Gomel, Belarus*

В статье показана реализация нового поляризатора циркулярно поляризованного излучения, основанного на использовании металлических двухспиральных (дс-) элементов массива и работающего при нормальном к оси спирали прохождении волны. Последнее обстоятельство является ключевым отличием данного массива от ряда аналогов, работающих на прохождение вдоль оси спирали. Приведено теоретическое обоснование поляризационной селективности дс-спиралей для перпендикулярного к оси направления прохождения излучения. Построена компьютерная модель для изучения электродинамических свойств массивов спиралей, которая подтвердила реализуемость циркулярного поляризатора для массива в СВЧ диапазоне длин волн.

Ключевые слова*: спираль, массив, поляризация, метаматериал.*

In this paper, we describe practical realization of a new type of circular polarizer based on metallic double-stranded (ds-) array particles, operating under normal to the helix axis wave propagation. The latter is the key distinction of this array from a number of analogous operating under propagation along the helix axis. Theoretical foundation of ds-helices polarization selectivity is given for a wave propagation perpendicular to the helix's axis. A computer model is created to study electrodynamic properties of arrays of helices, which confirms the circular polarizer feasibility for a microwave wavelength region.

Keywords: *helix, array, polarization, metamaterial.*

Introduction

In radio engineering there are several different ways to get circular microwaves by means of two-dimensional (2D) and three-dimensional (3D) metallic structures. One of the most widespread of them is the use of a spiral element. Although a helix can radiate in many modes, the axial mode and the normal mode present the common interest. The axial mode, the most commonly used mode, provides maximum radiation along the helix axis, which occurs when the helix circumference is of the order of one wavelength. The normal mode, which yields radiation broadside to the helix axis, occurs when the helix diameter is small as compared to a wavelength [1]. Typically, for a 3D helix, the flux of circular polarization is also radiated along the helix's axis, but a sidelobe polarization, if it exists, is not circular in general. This explains why the recent technique in developing helix-based circular polarizers is based on the along-helix-axis wave propagation [2]–[5]. In this article we propose a different approach for the circular polarizer realization, which is based on perpendicular to helix's axis wave propagation, but in this case the helix has a double stranded or bifilar structure with a specific shape and orientation in space. The parameters of helices as passive oscillators for perpendicular to helix axis wave propagation have been recently intensively studied by our group [6]–[11] and worldwide [12]–[14], this indicates high interest in this field of research.

1 Helix as a meta-atom particle

According to the Drude-Lorentz model, free electrons in metals can oscillate under the influence of external electromagnetic fields. The material properties of the metal become relevant to the field frequency. For metals with a curved shape, the possible oscillation trajectories are restricted by the curved surface of the metal. Therefore, free electrons have to follow the curvature of the metal surface. Harmonic external fields force the electrons to oscillate harmonically, therefore the electric current in the helix can be represented by a Fourier series

$$I(\phi, x) = \sum_{m=-\infty}^{m=\infty} I_m(x) e^{jm\phi},$$

where I_m is the amplitude of the *m*-harmonic, ϕ is the azimuth angle in the plane perpendicular to the helix axis, j is an imaginary unit. If the metal element has a periodic shape with its characteristic period corresponding to a wavelength, then a strong macro resonance of electric current can occur. For instance, consider a long metal single-stranded (ss-) helix,

fragment of which (1.5 turns or 3 half-turns) is depicted in Figure 1.1 (a). Theoretical analysis and computer modelling show that the main (principal) frequency resonance takes place when the wavelength approaches the period (length of one helix turn) of the helix $\lambda = P$. At this, the electric current has a harmonic mode, and, as it has been shown, it changes its direction every helix's half turn. No principal difference has been observed in the electric current distribution in the ds-helix [see Figure 1.1 (b)] in comparison to the ss-helix. There are, however, radical differences between these ss- and ds-helices in net electric $\mathbf{p} = \alpha_e E_\tau \boldsymbol{\tau}$ and magnetic $\mathbf{m} = \alpha_m E_n \mathbf{n}$ dipole responses induced in every half-turn(s) segment, where α_e, α_m are electric and magnetic polarizabilities of the segment, $\boldsymbol{\tau}$ is the unit vector directed along the wire, $\mathbf{n}$ is the unit vector directed normal to the wire loop plane, $E_{\tau,n}$ is the harmonic field of excitation. For chiral particles, however, both electric and magnetic fields are responsible for the dipole moments formation

$$\mathbf{p} = \varepsilon_0 \alpha_{ee} \mathbf{E} - j\sqrt{\varepsilon_0 \mu_0}\, \alpha_{em} \mathbf{H},$$

$$\mathbf{m} = \alpha_{mm} \mathbf{H} + j\sqrt{\varepsilon_0 / \mu_0}\, \alpha_{me} \mathbf{E},$$

where α_{ee} and α_{mm} are the tensors of dielectric and magnetic polarizabilities; α_{em} and α_{me} are the pseudotensors characterizing the chiral properties of the helix [15].

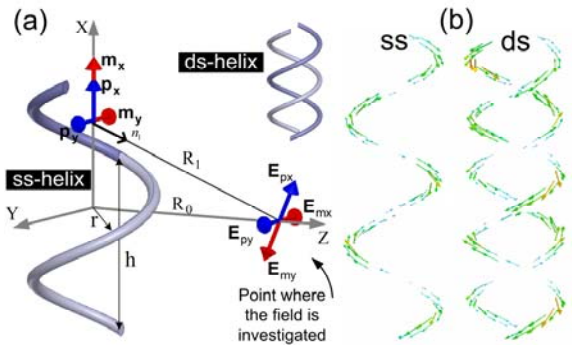

Figure 1.1 – (a) Schematic of the ss- and ds-helix where electric *p* and magnetic *m* responses are shown for the upper half-turn as well as the *E*-field induced by them, (b) surface electric current distribution along the 5 half-turn helices

Actually, due to the axial symmetry there are only axial dipoles for the ds-helix, but for the ss-one there are also perpendicular to axis dipoles, responsible for the helix scattering as well. The electric and magnetic moments induced in every half-turn of the ss-helix have been calculated. Important relations between them have been found

$$p_x = \frac{2j}{\omega r^2 q} m_x,$$

$$p_y \approx -\frac{2jq}{\omega} m_y,$$

$$p_z = m_z = 0,$$

where ω is the current cyclic frequency, $|q| = 2\pi / h$, we assume $q > 0$ and $q < 0$ for the right- and left-handed helices, respectively, and h is the helix pitch, r is the helix radius. These correlations of electric and magnetic moments were found for the main resonance electric current mode in Figure 1.1 (b).

Let us consider what helix shape is optimal for circularly polarized waves radiation in the perpendicular-to-axis direction [e. g. $\pm Z$ -axis in Figure 1.1 (a)], note that the helix's ends are located in the XY plane. Let us assume that the linearly polarized incident wave excites the helix in a perpendicular to its axis direction (e. g. propagates along $\pm Y$ -axis). The condition for radiation of a CP wave in the direction orthogonal to the helix axis [9] is the following

$$|p_x| = \frac{1}{c}|m_x|.$$

The discrete dipole radiation model is applied [16], which allows to calculate the instantaneous E -field gained from an individual half-turn(s). It can be done using the next formulas

$$\mathbf{E}_p = \frac{\mu_0}{4\pi R_0} (\ddot{\mathbf{p}}_i \times \mathbf{n}_i) \times \mathbf{n}_i,$$

$$\mathbf{E}_m = \frac{\mu_0}{4\pi c R_0} \mathbf{n}_i \times \ddot{\mathbf{m}}_i,$$

which are time and distance R_i dependent. Here $\mathbf{n}_i$ is a unit vector (see Figure 1.1 (a) for $i = 1$), c is the speed of light, double dots denote the 2nd time derivative [17]. In Figure1.1 (a) the total scattered field induced by the upper half-turn segment is shown in some point along the Z axis. We consider a monochromatic incident wave $e^{-j\omega t}$, therefore $\ddot{m} = -\omega^2 m$, $\ddot{p} = -\omega^2 p$. The resulting E -field can be calculated and the polarization of the radiated wave can be estimated by taking the sum of all field components from all half-turns. The ellipticity ε, which is of the great interest for polarization characterization, is introduced through the reciprocal axial ratio as defined for a general case in Ref. [18] as $\varepsilon = OA / OB$, where

$$OA = \left[\frac{1}{2}\left[E_x^2 + E_y^2 - \left[E_x^4 + E_y^4 + 2E_x^2 E_y^2 \cos(2\Delta\phi)\right]^{1/2}\right]\right]^{1/2},$$

$$OB = \left[\frac{1}{2}\left[E_x^2 + E_y^2 + \left[E_x^4 + E_y^4 + 2E_x^2 E_y^2 \cos(2\Delta\phi)\right]^{1/2}\right]\right]^{1/2}$$

here $\Delta\phi$ is the time-phase difference between the two components E_x and E_y of the field.

For the ds-helix, however, the ellipticity calculation is simplified to the axial ratio of components $\varepsilon = E_y / E_x$ as the phase difference between $\mathbf{p}$ and

m (and therefore $\mathbf{E}_p$ and $\mathbf{E}_m$) is $\pi/2$ and $\mathbf{E}_p$ is orthogonal to $\mathbf{E}_m$.

The following expressions were found for the components of the resulting electric field for the ss-helix

$$E_x \approx aR_0 \sum_{k=-N}^{N} \exp\left(j\omega \frac{R_k}{c} \right) \left\{ \frac{(-1)^{k+1} R_0}{R_k^3} p_x + \frac{1}{cR_k^2} m_y \right\},$$

$$E_y \approx a \sum_{k=-N}^{N} \exp\left(j\omega \frac{R_k}{c} \right) \left\{ \frac{1}{R_k} p_y + \frac{(-1)^{k+1} R_0}{cR_k^2} m_x \right\}$$

for the ds-helix they are

$$E_x = 2aR_0^2 p_x \sum_{k=-N}^{N} \frac{(-1)^{k+1}}{R_k^3} \exp\left(j\omega \frac{R_k}{c} \right),$$

$$E_y = \frac{2aR_0}{c} m_x \sum_{k=-N}^{N} \frac{(-1)^k}{R_k^2} \exp\left(j\omega \frac{R_k}{c} \right)$$

where R_0 is the distance between the origin and some point of field measuring (see Figure 1.1),

$$R_k = \sqrt{R_0^2 + \left(k \frac{h}{2} \right)^2}$$

is the distance from the half-turn with number k to the same point, and k is the index ranging from $-N$ to N,

$$a = \frac{\mu_0 \omega^2}{4\pi} \exp(-j\omega t).$$

We performed computer processing of the ellipticity to analyze the resultant polarization for short and long helices (with different N and R_0) in a far-field region. Usually a helix is characterized both by its radius r and pitch h, but they can be reduced to the helix pitch angle [19] via $\alpha = arc\cot(qr)$. It was found that the ellipticity results to unity only for the ds-helix with approximately $\alpha = 24.5°$ having only a weak dependence on N with the constant maximum position. A ss-helix can reach its maximum ellipticity of near 0.3 at more than doubled pitch angle in the far-field zone, which is not the same for the near-field zone.

2 Modelling of an individual particle

Using computer simulations we can confirm the key predictions of the proposed theoretical model. Parameters of the individual helical particle (as well as arrays of them) were modelled by the commercial software finite element method solver for electromagnetic structures Ansoft HFSS (High Frequency Structural Simulator) for optimal parameters search. We have investigated helices (both ss and ds) of different lengths in the range from 1 to 5 half-turn(s), but further discussion and an array realization is based on the results obtained for the 5 half-turn particle.

A monochromatic plane wave of 3 GHz propagated along the *Y*-axis and was able to excite the helix according to the model considered above. Simulations showed that the principal surface current mode induced in individual particles depicted in Figure 1.1 (b) is possible for a perpendicular to the helix axis direction of linear wave propagation having its *E*-vector oriented along the helix axis. The current has maximum in the center and the minimum at the ends of each half-turn. The field scattered by either ss- and ds- single particles along the *Z*-axis is investigated for the distance $R_0 = 10\lambda$. The results show a large difference in the axial ratios for the single ss- [see Figure 2.1 (a)] and ds-helix [see Figure 2.1 (b)], moreover, the phase difference $\Delta\varphi$ can reach $\pi/2$ for the ss-helix only at several spots (blue circles), but in wide regions for the ds-helix (solid curves).

Therefore, the unitary ellipticity is achievable for the latter case only. Resonance modes can be observed near the principal resonance $\nu_{res} = 3$ GHz. As it has been predicted by the theory, the highest value for the ellipticity is achieved at $\alpha = 55°$ for the ss-helix near the main resonance and at $\alpha = 20° - 30°$ for the ds-helix. Total scattered intensity can be calculated also from the proposed theoretical model and it is in agreement with the field strength peaks depicted in Figure 2.1.

As for single-layer arrays of ss-helices, the axial ratios can achieve high values, but the phase difference does not reach $\pi/2$ (pictures are not given). Ds-helix arrays behave much better in this way; we can compare differences induced by the change in orientation of the incident *E*-field of excitation: along the helix axis [see Figure 2.1 (c)] and perpendicular to it [see Figure 2.1 (d)]. One can see the regions where both the high axial ratio and $\Delta\varphi = \pi/2$ coexist (solid curve), which gives a circular polarization.

From the phase analysis of the $\mathbf{E}_p$, $\mathbf{E}_m$ oscillations we have found theoretically that the wave radiated by right-handed ds-DNA-like helix is polarized left-handed (DNA stands for deoxyribonucleic acid). To clarify, the *E*-vector of the wave follows a left-handed helix in space (very often this wave is called right-handed by engineers).

It is also important to study spatial distributions of scattered electromagnetic field (see Figure 2.2). These results showing strong narrow radiation beams along the *Z*-axis for ds-helices (in contrast to the ss-helices) are easy to understand taking into consideration the particle symmetry, its position in space and the perpendicular to the *Z*-axis maximal electric current direction, which contributes to the maximum radiation along this axis.

From the diagram in Figure 2.2 the advantage of ds-helices over ss-ones is obvious. In this picture, the difference between magnitudes of maximum and minimum scattered field is higher than one order.

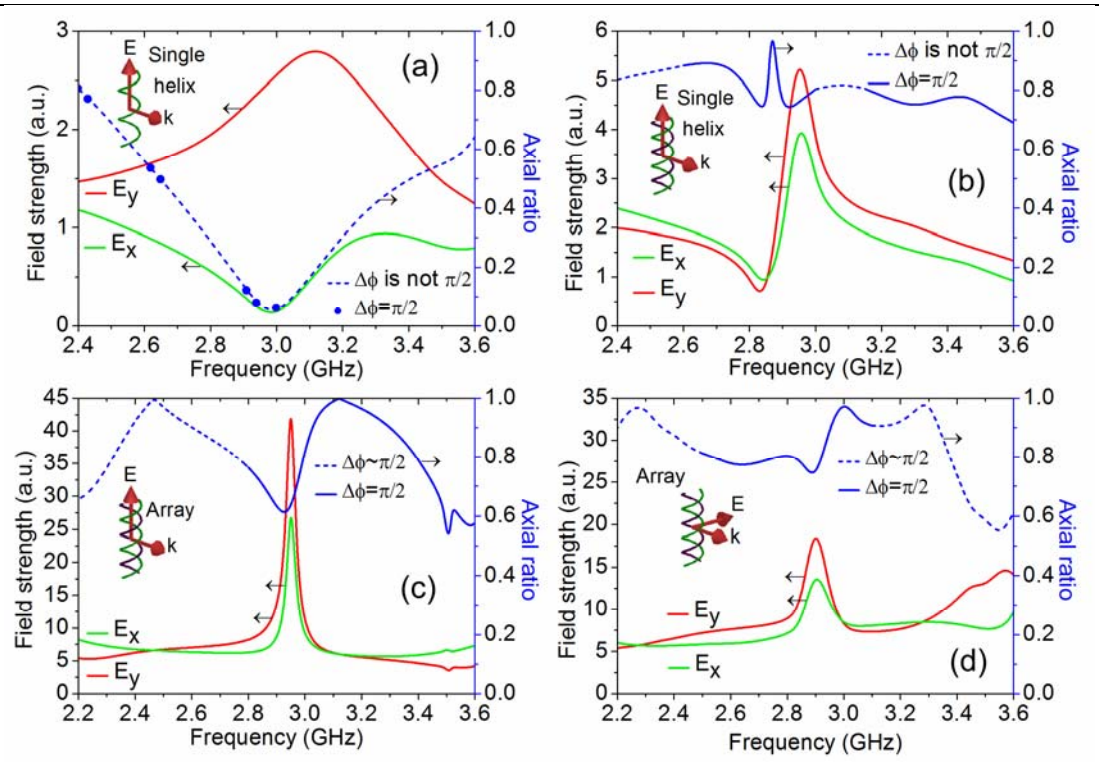

Figure 2.1 – (a), (b) Results of simulations: polarization analysis of the field scattered by the individual ss-helix (a) and the ds-helix (b). Incident linear wave propagates along the *Y*-axis (*E*-vector is along the helix axis), the *E*-field is detected at the point of the *Z*-axis at $R_0 = 10\lambda$; (c), (d) the field scattered by a single-layer array of ds-helices, when the incident linearly polarized wave propagates along the *Y*-axis, the *E*-vector is: along the *X*-axis (c), along the *Z*-axis (d)

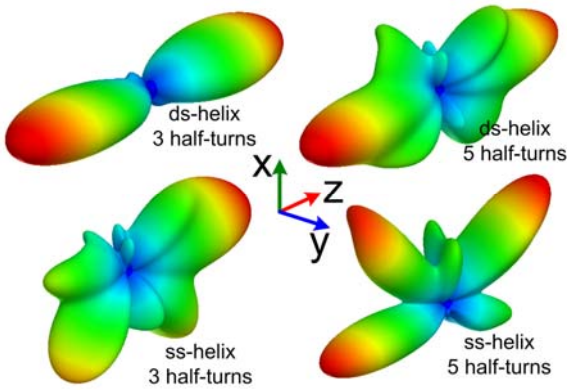

Figure 2.2 – Spatial distribution of the scattered electromagnetic field by the array of ds- and ss-helices of 3 and 5 half-turns. Vectors *k* and *E* of the incident linear wave were set along the *Y*- and *X*-axes, respectively

3 Three-dimensional arrays study for a circular polarizer realization

In this section we show how the mentioned advantage of ds-helices can be utilized for the development of 3D arrays acting as a circular polarizer. Incident circularly polarized wave is directed normally to one of the lateral surfaces of the array shown in Figure 3.1 (a). We study propagation of both right- and left-handed circularly polarized (RHCP, LHCP) waves, which are described by the following formula $\mathbf{e}_{\pm} = \frac{\mathbf{e}_1 \pm j\mathbf{e}_2}{\sqrt{2}}$, where $\mathbf{e}_1$, $\mathbf{e}_2$ are orthogonal unit vectors along the direction perpendicular to the wave vector.

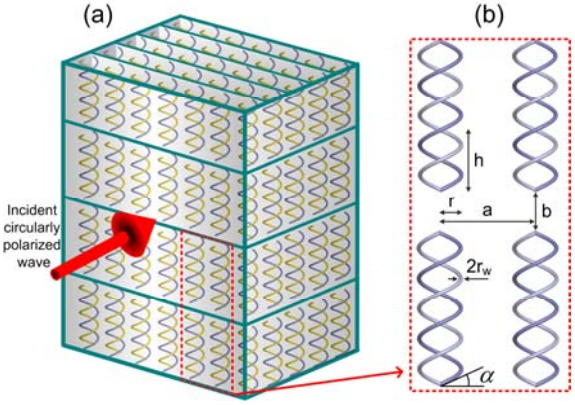

Figure 3.1 – (a) 3D array composed of metal ds-helices having the pitch angle of $\alpha = 24.5°$ and the incident circularly polarized radiation direction, (b) schematic of the array fragment with its parameters: the helix pith *h*=41.5 mm, the helix radius *r*=14.5 mm, the wire radius r_w=1 mm, the array parameters $a = 2\lambda/5$, $b = \lambda/5$, the inter-layer interval is $2\lambda/5$

The particles in the array are arranged so that their ends are placed in the plane formed by the incident wave vector and the helix axis. The lattice constant (the interval between the parallel layers) in the array is $2\lambda/5$, other parameters of the helix and the array are defined by Figure 3.1 (b) and have the following values: the helix pith h=41.5 mm, the helix radius r=14.5 mm, the wire radius r_w=1 mm, the array parameters $a=2\lambda/5$, $b=\lambda/5$, wavelength λ is 100 mm, the pitch angle is $\alpha = 24.5°$.

We studied the performance of the arrays as a polarization filter for a different number of layers in its composition. Far field analysis revealed clear peaks in spatial intensity and ellipticity diagrams. Figure 3.2 shows the total transmittance of electromagnetic radiation through a 5 layers array vs. frequency for different types of incident circularly polarized radiation – RHCP and LHCP. For low frequencies near the main frequency resonance, the interaction of the field with the helices is very strong and they scatter strongly perpendicular to the incident field direction, so the total propagation is very low. However, at higher frequencies, the effect of collective interaction between helices results in higher selective filtering of one circular mode than the opposite one. In our case, as the helices were right-handed, the propagation of RHCP mode is greater than for LHCP at wide frequency range between approximately 10 and 25 GHz. The study of the transmittance dependence on the number of layers in the array revealed the sharper transmittance peak for thicker arrays. This phenomenon can be explained in the following way. For an array with a small number of layers, strong lateral (relative to the direction of propagation) scattering takes place. For thicker array, this lateral scattering undergoes reflection towards the direction of propagation by further layers. Therefore, the resultant normally propagated intensity of radiation has higher and sharper profile in this case.

Propagated wave was predominantly RHCP (LHCP) polarized for RHCP (LHCP) incidence respectively. For more detailed analysis of the type of circular polarization of the propagated wave, we should assess the distinction ratio coefficient, which can be defined as

$$DR = \frac{T(\text{RHCP})}{T(\text{LHCP})},$$

where

$$T(\text{RHCP}) = \frac{I_{\text{tr}}^{\text{RHCP}}}{I_{\text{ic}}^{\text{RHCP}}},$$

$$T(\text{LHCP}) = \frac{I_{\text{tr}}^{\text{LHCP}}}{I_{\text{ic}}^{\text{LHCP}}}$$

are transmittances of the circular modes, *ic* denotes to incident field, *tr* denotes to transmitted field. From the *DR* coefficient (see Figure 3.2, black dashed curve) analysis one can see the array high transparency for RHCP radiation in comparison to LHCP radiation, what is expectable because the array is composed of right-handed helices. Thus, the performance of this array as a polarization filter (circularly polarized selective surface) and the circular polarizer is proved. The result of strong polarization interaction for a lower part of the considered frequency band was confirmed experimentally for mono-layered arrays elsewhere [20]. Moreover, similar effect takes place in pure dielectric photonic crystals [21], [22].

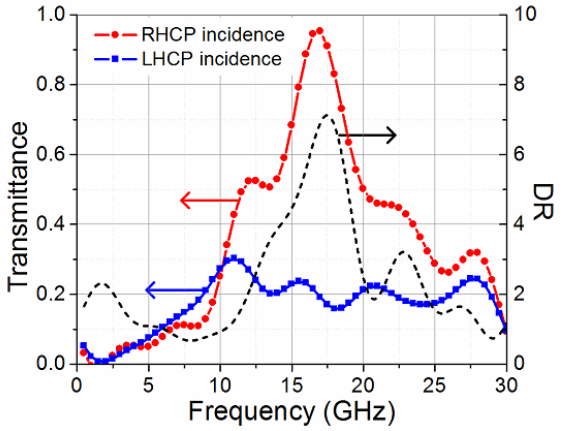

Figure 3.2 – Total transmittance vs. frequency for the array composed of 5 layers. Incident plane wave was circularly polarized, the red curve (circles) corresponds to the RHCP incidence radiation, the blue curve (squares) corresponds to the LHCP incidence radiation. The right scale and the black dashed curve represent the distinction ratio coefficient

Conclusion

We have realized a circular filter and polarizer for a non-typical – perpendicular to helix's axis – direction of wave propagation using the array composed of 5 layers of the ds-helices. This became possible due to the optimal helix shape and specific spatial arrangement of helices inside the array. This new type of array can also be applied to photonic crystals applications and therefore tends to be utilized in optics of infrared and visible light.

REFERENCES

1. *Volakis, J.L.* Antenna Engineering Handbook / J.L. Volakis. – 4th ed. – McGraw-Hill Co., 2007.

2. *Gold helix photonic metamaterial as broadband circular polarizer* / J.K. Gansel [et al.] // Science. – 2009. – Vol. 325. – P. 1513–1515.

3. *Gold helix photonic metamaterials: a numerical parameter study* / J.K. Gansel [et al.] // Optics Express. – 2010. – Vol. 18. – P. 1059–1069.

4. *Ultrabroadband optical circular polarizers consisting of double-helical nanowire structures* /

Z.Y. Yang [et al.] // Optics Letters. – 2010. – Vol. 35. – P. 2588–2590.

5. *Broadband terahertz circular polarizers with single- and double-helical array metamaterials* / S. Li [et al.] // Journal of the Optical Society of America A. – 2011. – Vol. 28. – P. 19–23.

6. *Semchenko, I.V.* Polarization selectivity of electromagnetic radiation of deoxyribonucleic acid / I.V. Semchenko, S.A. Khakhomov, A.P. Balmakov // Journal of Communications Technology and Electronics. – 2007. – Vol. 52. – P. 996–1001.

7. *Semchenko, I.V.* Cube Composed of DNA-like Helices Displays Polarization Selectivity Properties in Microwave / I.V. Semchenko, S.A. Khakhomov, A.P. Balmakov // in: Metamaterials 2009 – 3rd International Congress on Advanced Electromagnetic Materials in Microwaves and Optics. – London, UK – 2009. – P. 1–3.

8. *Semchenko, I.V.* Polarization Selectivity of Artificial Anisotropic Structures Based on DNA-Like Helices / I.V. Semchenko, S.A. Khakhomov, A.P. Balmakov // Crystallography Reports. – 2010. – Vol. 55. – P. 921–926.

9. *Semchenko, I.V.* Transformation of the polarization of electromagnetic waves by helical radiators / I.V. Semchenko, S.A. Khakhomov, A.L. Samofalov // Journal of Communications Technology and Electronics. – 2007. – Vol. 52. – P. 850–855.

10. *Semchenko, I.V.* Helices of optimal shape for nonreflecting covering / I.V. Semchenko, S.A. Khakhomov, A.L. Samofalov // The European Physical Journal Applied Physics. – 2010. – Vol. 49. – P. 33002.

11. *Khakhomov, S.A.* Advantages of metamaterials based on double-stranded DNA-like helices / S.A. Khakhomov [et al.] // in: Metamaterials'2012: The 6th International Congress on Advanced Electromagnetic Materials in Microwaves and Optics. – Saint Petersburg, 2012. – P. 1–3.

12. *Silveirinha, M.G.* Design of Linear-to-Circular Polarization Transformers Made of Long Densely Packed Metallic Helices / M.G. Silveirinha // IEEE Transactions on Antennas and Propagation. – 2008. – Vol. 56. – P. 390–401.

13. *Optically nonactive assorted helix array with interchangeable magnetic/electric resonance* / X. Xiong [et al.] // Applied Physics Letters. – 2011. – Vol. 98. – P. 071901.

14. *Metallic Helix Array as a Broadband Wave Plate* / C. Wu [et al.] // Physical Review Letters. – 2011. – Vol. 107. – P. 1–5.

15. *Electromagnetics of bi-Anisotropic Materials: theory and applications* / A. Serdyukov [et al.]. – Gordon and Breach, New York, 2001.

16. *Landau, L.D.* The Classical Theory of Fields / L.D. Landau, E.M. Lifshitz. – 4th ed. – Butterworth-Heinemann, 1980.

17. *Yavorsky, B.M.* Handbook of Physics / B.M. Yavorsky, A.A. Detlaf, N. Weinstein. – 4th ed. – Central Books Ltd., 1973.

18. *Balanis, C.A.* Antenna Theory / C.A. Balanis. – 2nd ed. – John Wiley and Sons, Inc., 1996.

19. *Semchenko, I.V.* Polarization selectivity of electromagnetic radiation of DNA / I.V. Semchenko, S.A. Khakhomov, A.P. Balmakov // in: Bianisotropics 2006 – International Conference on Complex Media and Metamaterials, 25–28 September 2006. – Samarkand, Uzbekistan, (printed in Helsinki University of Technology, Electromagnetics Laboratory, Espoo, Finland, Report 478). – P. 47–48.

20. *Семченко, И.В.* Взаимодействие искусственных ДНК-подобных структур в СВЧ диапазоне: поляризационная селективность отражения волн / И.В. Семченко, С.А. Хахомов, А.П. Балмаков // Радиофизика и электроника. – 2009. – Vol. 14. – P. 103–108.

21. *Three-dimensional horizontal circular spiral photonic crystals with stop gaps below 1 μm* / K.K. Seet [et al.] // Applied Physics Letters. – 2006. – Vol. 88. – P. 221101.

22. *Three-dimensional chiral photonic superlattices* / M. Thiel [et al.] // Optics Letters. – 2010. – Vol. 35. – P. 166–168.

Поступила в редакцию 15.11.12.